


## Article

# Structure and Electrical Properties of $\text{Na}_{0.5}\text{Bi}_{0.5}\text{TiO}_3$ Epitaxial Films with (110) Orientation

Jianmin Song <sup>1,2</sup>, Jie Gao <sup>2</sup>, Suwei Zhang <sup>3</sup> , Laihui Luo <sup>4</sup>, Xiuhong Dai <sup>1</sup>, Lei Zhao <sup>1,\*</sup> and Baoting Liu <sup>1,\*</sup>

<sup>1</sup> Hebei Key Lab of Optic-Electronic Information and Materials, College of Physics Science and Technology, Hebei University, Baoding 071002, China; sjm@hebau.edu.cn (J.S.); daixiuhong@hbu.edu.cn (X.D.)

<sup>2</sup> College of Science, Agriculture University of Hebei, Baoding 071001, China; jiegao1997@126.com

<sup>3</sup> Center for Advanced Measurement Science, National Institute of Metrology, Beijing 100029, China; zhangsw@nim.ac.cn

<sup>4</sup> College of Science, Ningbo University, Ningbo 315211, China; luolaihui@nbu.edu.cn

\* Correspondence: leizhao@hbu.edu.cn (L.Z.); btliao@hbu.edu.cn (B.L.)

Received: 17 September 2019; Accepted: 17 October 2019; Published: 25 October 2019



**Abstract:**  $\text{Pt}/\text{Na}_{0.5}\text{Bi}_{0.5}\text{TiO}_3/\text{La}_{0.5}\text{Sr}_{0.5}\text{CoO}_3$  ( $\text{Pt}/\text{NBT}/\text{LSCO}$ ) ferroelectric capacitors were fabricated on (110)  $\text{SrTiO}_3$  substrate. Both NBT and LSCO films were epitaxially grown on the (110)  $\text{SrTiO}_3$  substrate. It was found that the leakage current density of the  $\text{Pt}/\text{NBT}/\text{LSCO}$  capacitor is favorable to ohmic conduction behavior when the applied electric fields are lower than 60 kV/cm, and bulk-limited space charge-limited conduction takes place when the applied electric fields are higher than 60 kV/cm. The  $\text{Pt}/\text{NBT}/\text{LSCO}$  capacitor possesses good fatigue resistance and retention, as well as ferroelectric properties with  $P_r = 35 \mu\text{C}/\text{cm}^2$ . The ferroelectric properties of the  $\text{Pt}/\text{NBT}/\text{LSCO}$  capacitor can be modulated by ultraviolet light. The effective polarization,  $\Delta P$ , was reduced and the maximum polarization  $P_{\max}$  was increased for the  $\text{Pt}/\text{NBT}/\text{LSCO}$  capacitor when under ultraviolet light, which can be attributed to the increased leakage current density and non-reversible polarization  $P^+$  caused by the photo-generated carriers.

**Keywords:** NBT epitaxial film; ferroelectric properties; ultraviolet light

## 1. Introduction

Ferroelectric films are widely used in microelectromechanical systems, sensors and ferroelectric random access memory (FeRAM) due to their excellent dielectric, ferroelectric and piezoelectric properties [1–5]. The mainstay ferroelectric materials for applications have traditionally been the  $\text{Pb}(\text{Zr},\text{Ti})\text{O}_3$  (PZT) films due to their excellent performance (large remnant polarization  $P_r$  and small coercive field  $E_C$ ). However, the use of lead gives rise to environmental concerns, which is the driving force for the development of alternative lead-free ferroelectric materials [6–8].  $\text{Na}_{0.5}\text{Bi}_{0.5}\text{TiO}_3$  (NBT) with good ferroelectric properties and high Curie temperature has been considered to be an excellent candidate to replace lead-based ferroelectric materials [9–11]. Polycrystalline NBT films with  $P_r = 11.9 \mu\text{C}/\text{cm}^2$  have been grown on  $\text{Pt}/\text{Ti}/\text{SiO}_2/\text{Si}$  substrates [12]. It is believed that the highly oriented ferroelectric films (especially the epitaxial films) possess higher polarization than the polycrystalline ones due to the lack of grain boundaries. Highly (111) oriented NBT film prepared on  $\text{Pt}/\text{Ti}/\text{SiO}_2/\text{Si}$  substrate shows a higher  $P_r$  of  $20.9 \mu\text{C}/\text{cm}^2$  [13]. (001) and (011) oriented epitaxial NBT films fabricated on Pt-coated MgO and  $\text{SrTiO}_3$  substrates by pulsed laser deposition have good dielectric and ferroelectric properties [14,15]. In addition, both  $P_r$  and  $E_C$  are dependent on the crystal orientation. For example, the  $P_r$  and  $E_C$  are  $15.9 \mu\text{C}/\text{cm}^2$ ,  $12.6 \mu\text{C}/\text{cm}^2$  and 126 kV/cm, 94 kV/cm for (111) and (001) oriented NBT films [14,16].

The electrode materials are very important for ferroelectric capacitors. The noble metals, such as Pt, Au and Ag, are good electrode materials due to their excellent conductivity. However, the noble metals as bottom electrodes react easily with oxygen derived from the oxide films and deteriorate the performance of the oxide films [17]. Compared to Pt, Au and Ag, the  $\text{La}_{0.5}\text{Sr}_{0.5}\text{CoO}_3$  (LSCO) is low in cost and can provide an oxide/oxide (LSCO/NBT) interface that will not capture the oxygen from the oxide films [18,19]. In this work, Pt/NBT/LSCO ferroelectric capacitors were fabricated on (110)-oriented STO substrate by magnetron sputtering and pulsed laser deposition with LSCO as the bottom electrode. The microstructure and electrical properties of the Pt/NBT/LSCO ferroelectric capacitors, as well as the effect of ultraviolet light on the ferroelectric properties of these capacitors, were investigated.

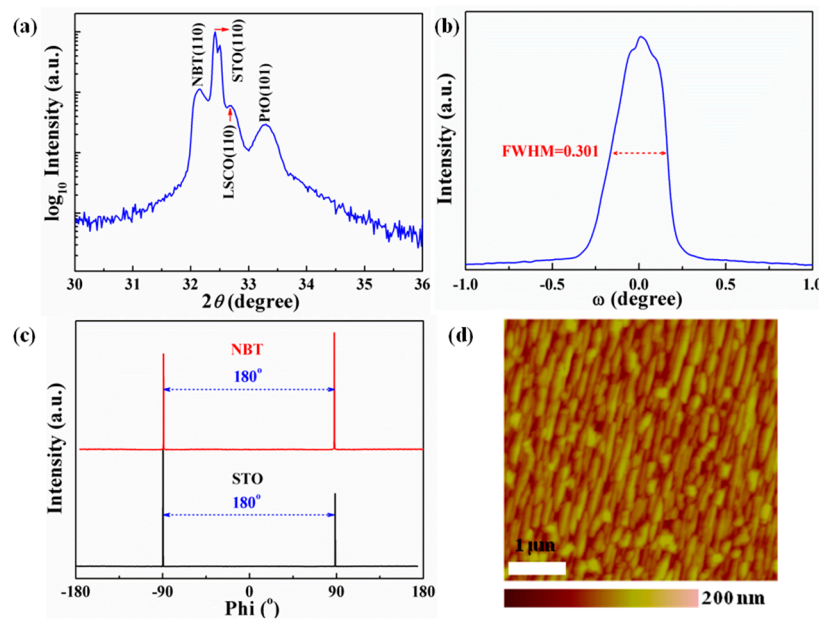
## 2. Experimental

The (110) oriented Pt/NBT/LSCO/STO heterojunction was prepared by magnetron sputtering and pulsed laser deposition. Step 1: LSCO film 60 nm in thickness was deposited on (110) STO single crystal substrate by magnetron sputtering at room temperature with the following conditions:  $\text{Ar}:\text{O}_2 = 3:1$ , power: 30 W. Post-annealing was conducted at 550 °C in a 1 atm oxygen-flowing tube furnace. The sheet resistance of the LSCO layer was  $20 \Omega/\square$ , which is quite low and would not affect the measurements. Step 2:  $\text{Na}_{0.5}\text{Bi}_{0.5}\text{TiO}_3$  target with excess 10% bismuth and 10% sodium was used to compensate the loss of bismuth and sodium. NBT film with a thickness of 400 nm was deposited on the LSCO/STO heterostructure by pulsed laser deposition at 550 °C and 7.5 Pa oxygen deposition pressure. The distance between the target and substrate was 5.5 cm; the laser energy density and repetition rate were  $2 \text{ J/cm}^2$  and 5 Hz, respectively. Step 3: Pt film with a thickness of 70 nm and an area of  $7.85 \times 10^{-5} \text{ cm}^2$  was deposited by magnetron sputtering on the surface of the NBT/LSCO/STO heterostructure through a shadow mask as the top electrodes of the capacitors. The Pt/NBT/LSCO/STO heterostructure was rapidly annealed at 550 °C for 1 min under an  $\text{O}_2$  atmosphere to make a better contact between the NBT and Pt.

The surface morphology of the (110) NBT film was measured by atomic force microscopy (AFM, MultiMode 8, Bruker, America). The phase structure was analyzed by X-ray diffractometer (XRD, TD-3700, Tongda, Dandong, China,  $\text{Cu K}\alpha$  radiation, tube pressure 30 kV, current 20 mA). The ferroelectric properties of Pt/NBT/LSCO capacitor were tested using a ferroelectric tester (Precision LC II, Radiant, America). The leakage current of the NBT film was tested using an I-V test system (2601B, Keithley, America). The ultraviolet light source (CEL-HXUV300, Zhongjiaojinyuan, Beijing, China) with 365 nm ( $5 \text{ mW/cm}^2$ ) was used.

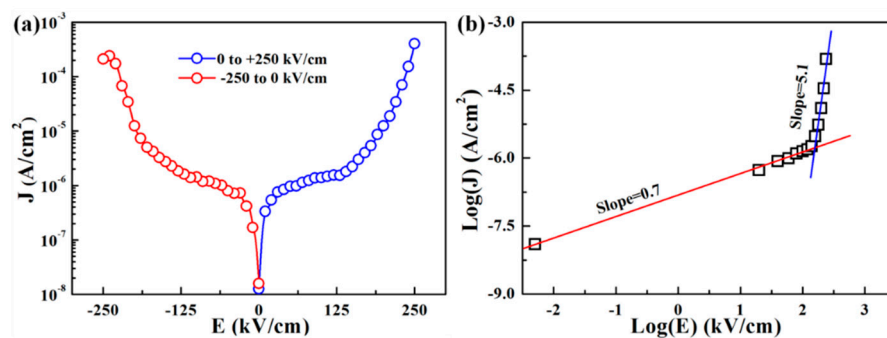
## 3. Results and Discussion

Figure 1a shows the XRD pattern of Pt/NBT/LSCO/STO heterojunction. In addition to the STO (110) peak, (110) diffraction peaks of NBT and LSCO are observed without any diffraction peaks from other directions, indicating that both NBT and LSCO films are highly (110) oriented. The full width at half maximum (FWHM) of the (110) diffraction peak for NBT film is  $0.301^\circ$  based on the rocking curve in Figure 1b, indicating high crystal quality. To further determine the epitaxial property of the NBT film, the phi-scan on the (100) plane of NBT film was performed as shown in Figure 1c. The two periodic diffraction peaks with similar intensity in the phi-scan further confirms that the NBT film is of good epitaxial nature. Figure 1d shows the surface topography of NBT film measured by AFM using tapping mode. It can be seen that the NBT film has a dense microstructure with a layered surface and elongated grains. The grain size is about 265 nm wide. The surface mean square roughness (RMS) is 15.5 nm, demonstrating that the NBT film has a highly crystalline quality. The elongated grain is consistent with that of the (110) oriented NBT film grown on the  $\text{SrTiO}_3$  substrate reported by Bousquet [15]. In addition, the appearance of PtO in XRD can be attributed to the reaction of Pt and  $\text{O}_2$ , since the sample was annealed at 550 °C for 1 min in  $\text{O}_2$  atmosphere.



**Figure 1.** (a) X-ray diffraction pattern of Pt/NBT/LSCO/STO heterojunction, in which the intensity of (110) STO is normalized; (b) Rocking curve of (110) diffraction peak for NBT film; (c) Phi scan and (d) AFM image of NBT film.

The leakage current density has a great impact on the electrical properties of the ferroelectric capacitors. Low current density is necessary for devices. Figure 2a shows the relationship between the leakage current density  $J$  and the electric field  $E$  for Pt/NBT/LSCO ferroelectric capacitor. The leakage current density is about  $4 \times 10^{-4}$  A/cm<sup>2</sup> and  $2 \times 10^{-4}$  A/cm<sup>2</sup> at 250 kV/cm and  $-250$  kV/cm, respectively. To further explore the conduction mechanisms of the Pt/NBT/LSCO capacitor in different electric field ranges, the leakage current curve was re-plotted as shown in Figure 2b. It was found that two mechanisms account for the leakage current characteristic of the Pt/NBT/LSCO capacitor. The  $\log(J)$  and  $\log(E)$  show a linear relation with a slope of 0.7 at 0~60 kV/cm, which is close to 1.0 and implies ohmic-like conduction [20,21]. There are a small number of carriers generated by thermal excitation in the NBT film, which contributes to the low  $J$  at 0~60 kV/cm. The nonlinear space-charge current-limiting mechanism is responsible for the higher  $J$  at 60~250 kV/cm. The Fermi energy is different for LSCO and Pt, which would cause a large Schottky barrier in the interfaces. A large number of electrons gathered in the electrodes under  $E$ . These electrons are activated when  $E$  is higher than the potential well and enter the NBT film to form leakage current. Thus,  $J$  increased sharply.



**Figure 2.** Leakage current density *vs.* applied electric fields (a) and  $\log(J)$  *vs.*  $\log(E)$  (b) for (110) NBT film.

Figure 3a shows the P-E loops of (110) NBT film at different  $E$  under 10 kHz. (110) NBT film shows typical ferroelectric P-E loops. Both  $P_r$  and  $P_{max}$  increase with  $E$ . The saturated  $P_r$  of the (110) NBT film

is about  $35 \mu\text{C}/\text{cm}^2$ , indicating good ferroelectric properties. The  $P_r$  of NBT ceramic is  $38.0 \mu\text{C}/\text{cm}^2$  [22]. In cubic structure, the angle between the (110) and (111) planes is  $35.26^\circ$ . In theory,  $P_r = \cos(35.26^\circ) \times 38.0 \mu\text{C}/\text{cm}^2 \approx 31.0 \mu\text{C}/\text{cm}^2$  by assuming the polarization vector is along the [111] direction. The saturated  $P_r$  of (110) NBT film is  $35 \mu\text{C}/\text{cm}^2$ , which is higher than that ( $P_r = 31.0 \mu\text{C}/\text{cm}^2$ ) of the NBT ceramic in (110) orientation. The increased  $P_r$  in (110) NBT film can be attributed to the pressure stress caused by the lattice mismatch in the NBT/LSCO interface. In the Pt/NBT/LSCO heterojunction, the in-plane lattice parameter  $a$  is  $0.389 \text{ nm}$  and  $0.383 \text{ nm}$  for NBT and LSCO based on the XRD pattern. The different lattice parameter  $a$  would lead to pressure stress and an enlarged  $c/a$  ratio (the out-of-plane lattice parameter  $c$  to the in-plane lattice parameter  $a$ ) in the NBT film. The relationship between the saturation polarization  $P_s$  and  $c/a$  is  $(P_s)^2 \propto (c/a-1)^2$  in ferroelectric materials [23]. Thus, the pressure stress caused by the lattice mismatch will increase the polarization of the (110) NBT film.

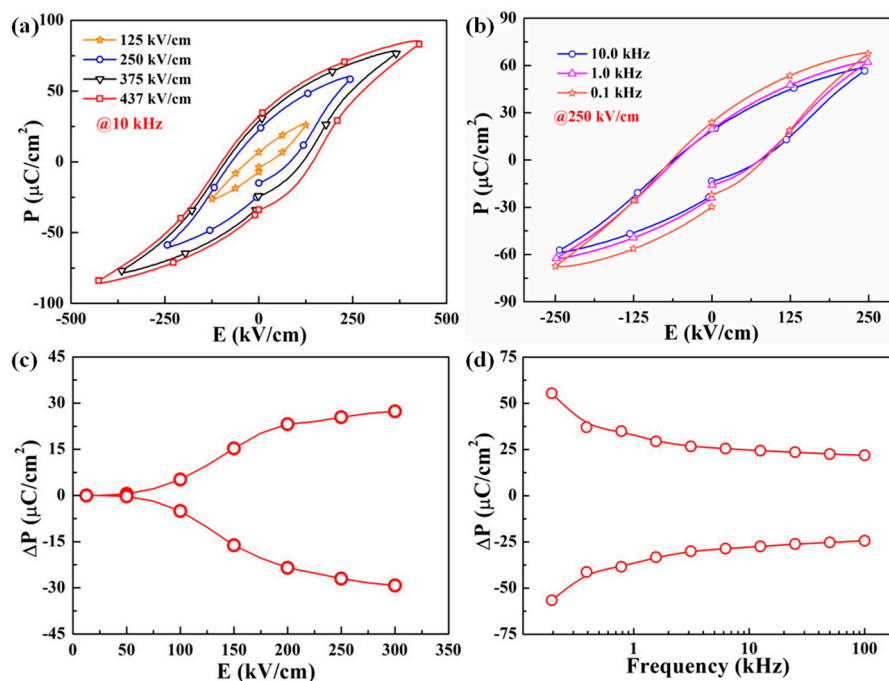


**Figure 3.** Electric field and frequency dependence of hysteresis loops (a,b) and  $\Delta P$  (c,d) for (110) NBT film.

The dependence of P-E loops on the frequency under  $250 \text{ kV/cm}$  was depicted in Figure 3b. The P-E loops of (110) NBT film become weak with increasing frequency from  $0.1 \text{ kHz}$  to  $10 \text{ kHz}$ . This may be due to the fact that the domain cannot be completely reversed at high frequencies, which leads to a decrease in the polarization. The effective polarization  $\Delta P$  ( $\Delta P = P^* - P^\wedge$ ,  $P^*$  is the reversible polarization,  $P^\wedge$  is the non-reversible polarization) can remove the influence of leakage current and is an important parameter for ferroelectric memories. Figure 3c is the dependence of  $\Delta P$  on  $E$ . When  $E$  is  $0\text{--}50 \text{ kV/cm}$ ,  $\Delta P$  remains unchanged.  $\Delta P$  rapidly increases with  $E$  as  $E$  is higher than  $50 \text{ kV/cm}$  and gradually becomes saturated as  $E$  is over  $175 \text{ kV/cm}$ . At  $200 \text{ kV/cm}$ ,  $\Delta P$  is  $20.3 \mu\text{C}/\text{cm}^2$ . The slightly increased  $\Delta P$  as  $E > 200 \text{ kV/cm}$  indicates that the ferroelectric domain may be completely inverted. Figure 3d is the dependence of  $\Delta P$  on the frequency. The  $\Delta P$  declines nonlinearly with the increase of frequency since the ferroelectric domains do not have enough time to inverse at high frequencies, which leads to reduced  $P^*$ . As the frequency is higher than  $1 \text{ kHz}$ ,  $\Delta P$  shows weaker dependence on the frequency, indicating faster access speed.

The fatigue of the Pt/NBT/LSCO capacitor was tested at 250 kV/cm and 1 MHz, as shown in Figure 4a. No obvious degradation in  $\Delta P$  can be found for the LSCO bottom electrode. However, the  $\Delta P$  reduced to  $13.5 \mu\text{C}/\text{cm}^2$  from  $16.5 \mu\text{C}/\text{cm}^2$  after  $10^{10}$  switching cycles for the Pt top electrode. These results indicate that the LSCO bottom electrode is good for fatigue resistance and the Pt top electrode would cause decreased  $\Delta P$  due to the reaction of Pt and O from NBT film [18,19]. The inset of Figure 4a presents the P-E loops before and after  $10^{10}$  switching cycles, in which a decreased P-E loop was observed. Figure 4b is the retention of the Pt/NBT/LSCO capacitor. There is no obvious degradation in  $\Delta P$  for either electrode after  $10^4$  s, indicating that the Pt/NBT/LSCO capacitor has good retention characteristics. In addition, the similar P-E loops before and after  $10^4$  s shown in the inset of Figure 4b further confirm the good retention characteristics. It seems that the retention characteristic is independent on the electrode materials.

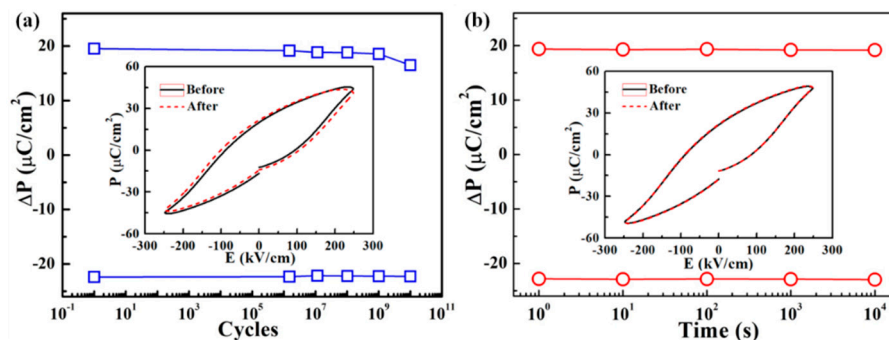


**Figure 4.** Fatigue (a) and retention (b) of Pt/NBT/LSCO capacitor. The insets are the hysteresis loops before and after  $10^{10}$  switching cycles (a) and  $10^4$  s (b).

To investigate the effect of light on the ferroelectric properties of the Pt/NBT/LSCO capacitor, ultraviolet light with a wavelength of 365 nm was used, since the forbidden gap of NBT film is 3.15 eV, as shown in Figure 5a. Figure 5b shows the P-E loops of the Pt/NBT/LSCO capacitor under dark and ultraviolet light. It can be seen that the  $P_{\text{max}}$  is  $60.6 \mu\text{C}/\text{cm}^2$  and  $63.8 \mu\text{C}/\text{cm}^2$  under dark and ultraviolet light, respectively, indicating that the ultraviolet light can increase the polarization of the Pt/NBT/LSCO capacitor.  $P_{\text{max}}$  ( $P_{\text{max}} = 2\Delta P + Jt$ ,  $\Delta P$  is effective polarization,  $J$  is leakage current density and  $t$  is time) can be affected by  $\Delta P$  and  $J$ . Under ultraviolet light, photo-generated carriers would be generated in NBT film, increasing  $J$ , and thus causing an increase in  $P_{\text{max}}$ . To further illustrate the effect of ultraviolet light on  $\Delta P$ , the dependences of  $\Delta P$  on  $E$  and frequency under ultraviolet light were investigated as shown in Figure 5c,d. It can be seen that the ultraviolet light leads to reduced  $\Delta P$ . This is attributed to the increased  $P^*$  caused by the ultraviolet light. The decreased  $\Delta P$  further confirms that the increased  $P_{\text{max}}$  can be attributed to the increased  $J$  under ultraviolet light. The ultraviolet light leads to decreased  $\Delta P$ , but does not change the tendencies of  $\Delta P$  with  $E$  and frequency. Based on the analysis described above, it can be concluded that the increased  $P_{\text{max}}$  in the Pt/NBT/LSCO capacitor is due to the increased  $J$  caused by the photo-generated carriers rather than the increased  $\Delta P$ .



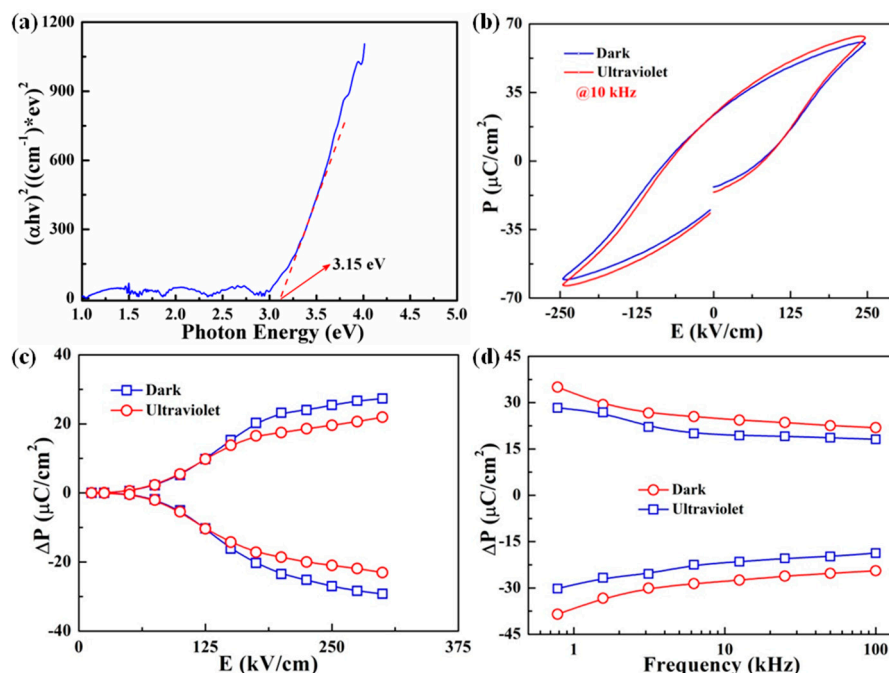


**Figure 5.** Forbidden gap (a), hysteresis loops (b), electric field-dependence (c) and frequency-dependence (d) of  $\Delta P$  for Pt/NBT/LSCO capacitor under ultraviolet light.

#### 4. Conclusions

The Pt/NBT/LSCO capacitor was fabricated on (110) STO substrate by magnetron sputtering and pulsed laser deposition with LSCO as the bottom electrode. The microstructure and electrical properties of the (110) oriented NBT film were investigated. It was found that the (110) oriented NBT/LSCO films were epitaxially grown on  $\text{SrTiO}_3$  substrate with high crystal quality. The (110) NBT film shows good ferroelectric properties, with  $P_r = 35 \mu\text{C}/\text{cm}^2$  and a small leakage current density of  $4.02 \times 10^{-4} \text{ A}/\text{cm}^2$  at 250 kV/cm. The ohmic conduction mechanism and nonlinear space charge limiting accounted for the conduction mechanisms at 0–60 kV/cm and 60–250 kV/cm, respectively. The  $\Delta P$  of the Pt/NBT/LSCO capacitor shows strong dependence on both the electric field and frequency. In addition, the Pt/NBT/LSCO capacitor processes good fatigue resistance and retention. The ultraviolet light leads to increased leakage current density and non-reversible polarization  $P^*$ , and causes reduced  $\Delta P$  and increased  $P_{\text{max}}$ . These results can provide a reference for the research and development of lead-free NBT ferroelectric storage devices.

**Author Contributions:** J.S. and J.G. contributed equally to this work in sample preparation and testing. S.Z. worked for data analysis and English. L.L. and X.D. worked for data analysis. L.Z. and B.L. worked for manuscript writing.

**Funding:** This research received no external funding.

**Acknowledgments:** This project is supported by the National Natural Science Foundation of China (Grant numbers 11374086 and 51802068), the Natural Science Foundation of Hebei Province (Grant numbers E2014201188, E2014201063 and A2018201168), the Advanced Talents Incubation Program of Hebei University (Grant numbers 801260201180 and 521000981323) and the State Key Laboratory of New Ceramic and Fine Processing Tsinghua University (Grant number KF201812).

**Conflicts of Interest:** The authors declare no conflict of interest.

## References

- Peddigari, M.; Palneedi, H.; Hwang, G.T.; Lim, K.W.; Kim, G.Y.; Jeong, D.Y.; Ryu, J. Boosting the Recoverable Energy Density of Lead-Free Ferroelectric Ceramic Thick Films through Artificially Induced Quasi-Relaxor Behavior. *ACS Appl. Mater. Interfaces* **2018**, *10*, 20720–20727. [[CrossRef](#)]
- Tang, Z.; Liu, Z.; Ma, J.; Fan, J.; Zhong, M.; Tang, X.G.; Lu, S.G.; Tang, M.; Gao, J. The enhanced magnetoelectric effect and piezoelectric properties in the lead-free  $\text{Bi}_{3.15}\text{Nd}_{0.85}\text{Ti}_3\text{O}_{12}/\text{La}_{0.7}\text{Ca}_{0.3}\text{MnO}_3$  nano-multilayers composite thin films. *J. Alloys Compd.* **2019**, *777*, 485–491. [[CrossRef](#)]
- Wen, Z.; Li, C.; Wu, D.; Li, A.; Ming, N. Ferroelectric-field-effect-enhanced electroresistance in metal/ferroelectric/semiconductor tunnel junctions. *Nat. Mater.* **2013**, *12*, 617–621. [[CrossRef](#)]
- Tian, B.B.; Liu, Y.; Chen, L.F.; Wang, J.L.; Sun, S.; Shen, H.; Sun, J.L.; Yuan, G.L.; Fusil, S.; Garcia, V.; et al. Space-charge Effect on Electroresistance in Metal-Ferroelectric-Metal capacitors. *Sci. Rep.* **2015**, *5*, 18297. [[CrossRef](#)] [[PubMed](#)]
- Abuwasib, M.; Lu, H.; Li, T.; Buragohain, P.; Lee, H.; Eom, C.B.; Gruverman, A.; Singiseti, U. Scaling of electroresistance effect in fully integrated ferroelectric tunnel junctions. *Appl. Phys. Lett.* **2016**, *108*, 152904. [[CrossRef](#)]
- Zhang, T.; Li, W.; Cao, W.; Hou, Y.; Yu, Y.; Fei, W. Giant electrocaloric effect in PZT bilayer thin films by utilizing the electric field engineering. *Appl. Phys. Lett.* **2016**, *108*, 162902. [[CrossRef](#)]
- Katsouras, I.; Asadi, K.; Groen, W.A.; Blom, P.W.M.; De Leeuw, D.M.; Zhao, D. Retention of intermediate polarization states in ferroelectric materials enabling memories for multi-bit data storage. *Appl. Phys. Lett.* **2016**, *108*, 232907. [[CrossRef](#)]
- Gobeljic, D.; Shvartsman, V.V.; Belianinov, A.; Okatan, B.; Jesse, S.; Kalinin, S.V.; Groh, C.; Rödel, J.; Lupascu, D.C.; Okatan, M.; et al. Nanoscale mapping of heterogeneity of the polarization reversal in lead-free relaxor–ferroelectric ceramic composites. *Nanoscale* **2016**, *8*, 2168–2176. [[CrossRef](#)] [[PubMed](#)]
- Smolenskii, G.A.; Isypov, V.A.; Agranovskaya, A.I.; Krainik, N.N. New ferroelectrics complex composition. *Sov. Phys. Solid State* **1961**, *2*, 2651–2654.
- Cao, W.; Li, W.; Feng, Y.; Bai, T.; Qiao, Y.; Hou, Y.; Zhang, T.; Yu, Y.; Fei, W. Defect dipole induced large recoverable strain and high energy-storage density in lead-free  $\text{Na}_{0.5}\text{Bi}_{0.5}\text{TiO}_3$ -based systems. *Appl. Phys. Lett.* **2016**, *108*, 202902. [[CrossRef](#)]
- Balakt, A.; Shaw, C.; Zhang, Q. Enhancement of pyroelectric properties of lead-free  $0.94\text{Na}_{0.5}\text{Bi}_{0.5}\text{TiO}_3$ - $0.06\text{BaTiO}_3$  ceramics by La doping. *J. Eur. Ceram. Soc.* **2017**, *37*, 1459–1466. [[CrossRef](#)]
- Zhou, Z.H.; Xue, J.M.; Li, W.Z.; Wang, J.; Zhu, H.; Miao, J.M. Leakage current and charge carriers in  $(\text{Na}_{0.5}\text{Bi}_{0.5})\text{TiO}_3$  thin film. *J. Phys. D Appl. Phys.* **2005**, *38*, 642–648. [[CrossRef](#)]
- Tang, X.G.; Wang, J.; Wang, X.X.; Chan, H.L.W. Preparation and Electrical Properties of Highly (111)-Oriented  $(\text{Na}_{0.5}\text{Bi}_{0.5})\text{TiO}_3$  Thin Films by a Sol–Gel Process. *Chem. Mater.* **2004**, *16*, 5293–5296. [[CrossRef](#)]
- Bousquet, M.; Duclère, J.-R.; Champeaux, C.; Boulle, A.; Marchet, P.; Catherinot, A.; Wu, A.; Vilarinho, P.M.; Députier, S.; Guilloux-Viry, M.; et al. Macroscopic and nanoscale electrical properties of pulsed laser deposited (100) epitaxial lead-free  $\text{Na}_{0.5}\text{Bi}_{0.5}\text{TiO}_3$  thin films. *J. Appl. Phys.* **2010**, *107*, 034102. [[CrossRef](#)]
- Bousquet, M.; Duclère, J.-R.; Gautier, B.; Boulle, A.; Wu, A.; Deputier, S.; Fasquelle, D.; Rémondière, F.; Albertini, D.; Champeaux, C.; et al. Electrical properties of (110) epitaxial lead-free ferroelectric  $\text{Na}_{0.5}\text{Bi}_{0.5}\text{TiO}_3$  thin films grown by pulsed laser deposition: Macroscopic and nanoscale data. *J. Appl. Phys.* **2012**, *111*, 104106. [[CrossRef](#)]
- Duclère, J.-R.; Cibert, C.; Boulle, A.; Dorcet, V.; Marchet, P.; Champeaux, C.; Catherinot, A.; Deputier, S.; Guilloux-Viry, M. Lead-free  $\text{Na}_{0.5}\text{Bi}_{0.5}\text{TiO}_3$  ferroelectric thin films grown by Pulsed Laser Deposition on epitaxial platinum bottom electrodes. *Thin Solid Films* **2008**, *517*, 592–597. [[CrossRef](#)]
- Solbach, A.; Klemradt, U.; Schorn, P.J.; Böttger, U.; Cao, J.L.; Weirich, T.E.; Mayer, J. Probing fatigue in ferroelectric thin films with subnanometer depth resolution. *Appl. Phys. Lett.* **2007**, *91*, 72905.
- Liu, B.T.; Chen, J.E.; Sun, J.; Wei, D.Y.; Chen, J.H.; Li, X.H.; Bian, F.; Zhou, Y.; Guo, J.X.; Zhao, Q.X.; et al. Oxygen vacancy as fatigue evidence of  $\text{La}_{0.5}\text{Sr}_{0.5}\text{CoO}_3/\text{PbZr}_{0.4}\text{Ti}_{0.6}\text{O}_3/\text{La}_{0.5}\text{Sr}_{0.5}\text{CoO}_3$  capacitors. *EPL Europhys. Lett.* **2010**, *91*, 67011. [[CrossRef](#)]
- Song, J.M.; Luo, L.H.; Dai, X.H.; Song, A.Y.; Zhou, Y.; Li, Z.N.; Liang, J.T.; Liu, B.T. Switching properties of epitaxial  $\text{La}_{0.5}\text{Sr}_{0.5}\text{CoO}_3/\text{Na}_{0.5}\text{Bi}_{0.5}\text{TiO}_3/\text{La}_{0.5}\text{Sr}_{0.5}\text{CoO}_3$  ferroelectric capacitor. *RSC Adv.* **2018**, *8*, 4372–4376. [[CrossRef](#)]

20. Cheng, B.L.; Wang, C.; Zhou, Y.L.; Wang, S.Y.; Dai, S.Y.; Lu, H.B.; Chen, Z.H.; Yang, G.Z. Reduction of leakage current by Co doping in Pt/Ba<sub>0.5</sub>Sr<sub>0.5</sub>TiO<sub>3</sub>/Nb–SrTiO<sub>3</sub> capacitor. *Appl. Phys. Lett.* **2004**, *84*, 4116.
21. Qi, Y.; Lu, C.; Zhang, Q.; Wang, L.; Chen, F.; Cheng, C.; Liu, B. Improved ferroelectric and leakage properties in sol–gel derived BiFeO<sub>3</sub>/Bi<sub>3.15</sub>Nd<sub>0.85</sub>Ti<sub>3</sub>O<sub>12</sub> bi-layers deposited on Pt/Ti/SiO<sub>2</sub>/Si. *J. Phys. D Appl. Phys.* **2008**, *41*, 065407. [[CrossRef](#)]
22. Hiruma, Y.; Nagata, H.; Takenaka, T. Thermal depoling process and piezoelectric properties of bismuth sodium titanate ceramics. *J. Appl. Phys.* **2009**, *105*, 084112. [[CrossRef](#)]
23. Fatuzzo, E.; Merz, W.J. *Ferroelectricity*; North-Holland Publishing Company: Amsterdam, The Netherlands, 1967.



© 2019 by the authors. Licensee MDPI, Basel, Switzerland. This article is an open access article distributed under the terms and conditions of the Creative Commons Attribution (CC BY) license (<http://creativecommons.org/licenses/by/4.0/>).